Metal fuels production through the solar carbothermal reduction of magnesia: Effect of the reducing agent

Youssef Berro, Damaris Kehrli, Jean-François Brilhac, Marianne Balat-Pichelin

Metal fuels production through the solar carbothermal reduction of magnesia: Effect of the reducing agent

Youssef Berro [a], Damaris Kehrli [b], Jean-François Brilhac [b], Marianne Balat-Pichelin [a] *

[a] Laboratoire PROcédés, Matériaux et Energie Solaire, PROMES-CNRS, UPR 8521, 7 rue du four solaire, 66120 Font-Romeu Odeillo, France.

[b] Laboratoire Gestion des Risques et Environnement, LGRE-UHA UR 2334, Université de Haute-Alsace, 3bis rue Alfred Werner, 68093 Mulhouse, France.

*corresponding author: marianne.balat@promes.cnrs.fr

Abstract

The use of metallic powders as substitute combustion fuels for transportation gains much interest due to their high energetic value, the absence of greenhouse gas emissions, and the ability to regenerate them. Herein, we studied their production through the carbothermal reduction (CTR) of magnesia in the Sol@rmet reactor, at low pressure, using concentrated solar power (CSP) and different charcoal reducing agents as sustainable sources. Previous kinetic studies suggested that the C/MgO phase boundary reaction is the dominant phase at the initial stage of reduction. Additionally, one of the main problems encountered at high temperatures is the sintering of MgO particles, which reduces their contact with carbon and in consequence the reduction rate. Thus, we investigated the effect of the charcoal reducing agent properties (source, pyrolysis conditions, C-content…) and bentonite binder on the metallic conversion. Experimental results proved the catalytic-like role of bentonite binder giving values up to 95% of Mg yield and purity during the gradual increase of the temperature using a charcoal with high fixed carbon content of 94%.

Keywords: carbothermal reduction (CTR), magnesia, solar fuels, charcoal, bentonite.

1. Introduction

Nowadays, efforts are cumulated to confront the depletion of fossil fuels and the global warming.[1] In this context, the United Nations admitted a resolution to ensure clean and sustainable energy, and to combat the climate change.[2] In 2010, road transport accounts for around 10% of the global greenhouse gases (GHGs), and this contribution increases in the developing countries.[3] Thus, in the 20th century, intense research focused on the use of sustainable fuel sources in the transport field and on developing environmental-friendly cars.

In 2015, Bergthorson *et al.*[4] proposed an innovative process for the regeneration of recyclable metal fuels, as promising zero-carbon energy-carrying materials having high energy densities,[5] to improve the sustainability of the energy/fuel cycle. The process consists of the direct combustion of those fuels in a metal-fueled combustor with the ability to collect the combustion oxide products and regenerate the metallic fuels using renewable energy sources as shown in **Figure 1**. A review research highlighted this process by discussing the combustion modes of the metal powders, the stabilization of the metal fuel flame, and the development of metal-fueled engines to be used for clean power generation.[4,6] More recently, a collaboration project between STELLANTIS group and ICARE-CNRS treated the development of a new metal-fueled engine for cars.[7] They published several studies investigating the combustion of metal fuels in a burner under a stable flame, the improvement of the burning time and the collection of metal oxide to regenerate them.[8,9] An innovative power generation system where 50-70 μm magnesium particles are combusted in a swirled-stabilized metal-air burner has been developed in a collaborative work between STELLANTIS and LGRE-UHA[10] and 98% of the produced submicron magnesia particles are trapped and collected.[11] This system proved to have an optimal heat-to-mechanical conversion efficiency where 80% of the power generated from combustion is recovered in the power generation system.[12]

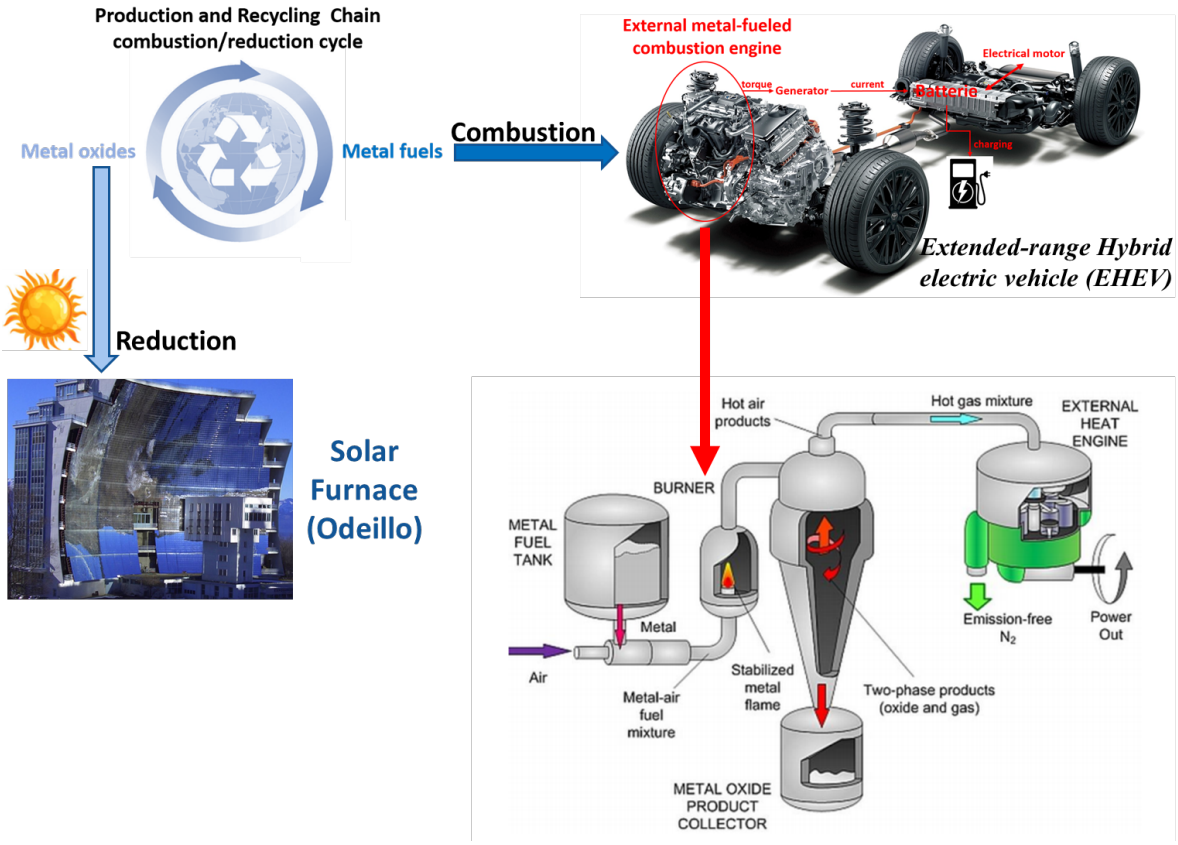

Figure 1. *Production and recycling chain of metal fuels through combustion/reduction cycles for a sustainable circular economy (metal-fueled reactor from Bergthorson et al.[4]).*

The regeneration of magnesium fuels can be achieved through the reduction of the combustion product, magnesia, using concentrated solar power (CSP) as a sustainable heating source. In this context, various researchers around the world probed the solar reduction of different metal oxides, mainly at the University of Minnesota (USA),[13] PSI and ETH Zurich (Switzerland),[14] PROMES-CNRS (France),[15] IMDEA Energy (Spain),[16] WIS (Israel),[17] and DLR-German Aerospace center (Germany).[18] The reduction can be assisted using carbon reducing agent as the onset temperature of the reaction decreases from 3700 to 2130 K.[19,20] Those findings motivated Puig and Balat-Pichelin[21] to study the solar carbothermal reduction of magnesia, as a recycling process of Mg metallic fuels, proving that operating under low pressures reduces the required temperature of the reaction and improves the reduction rate.[21] Under those conditions, investigating the reaction kinetics suggests that, at low temperatures

($T < 1750$ K) and conversation rate ($X_{MgO} = 0.2$), the reaction correlates well with the C/MgO solid phase-boundary reaction with an activation energy of around 208 kJ mol^{-1}. Whereas, at higher temperatures and conversion rates, magnesia is mainly reduced by CO due to the loss of the C/MgO contact that may be caused by the decrease of the reactants surface area, the MgO sintering,[22] and the MgO densification.[23] In this case, the reaction is a solid-gas reaction having a higher activation energy of about 374 kJ mol^{-1}.[22,23] In fact, the reaction kinetics are highly dependent on the reaction pressure as the activation energy rises from around 200 kJ·mol^{-1} at 100-1000 Pa (phase boundary reaction) to 325 kJ mol^{-1} at 10^4-10^5 Pa, meaning that the rate-determining step of the reaction has changed as the influence of the solid-gas reaction is more important at higher pressures.[22] Under vacuum, the CO partial pressure is reduced and thus the gas-solid reaction is limited, which promotes the solid-solid interface reaction.[24] Thus, the carbon properties are the main parameters that determine the reaction kinetics by reducing or extending the duration of the phase boundary reaction.

Another problematic to consider during the magnesia carbothermal reduction is the possible re-oxidation of the Mg particles through the reverse CO/Mg reaction, during the condensation phase, which reduces the powders purity.[25] However, under low vacuum conditions and CO partial pressure ($P_{CO} < 300$ Pa), the magnesium vapor pressure is reduced allowing its rapid condensation at temperatures lower than 973 K (condensation rate becomes faster than the oxidation rate) and yielding high purity powders (> 90%).[24,25] Vishnevetsky *et al.*[17,26] proved that, during the solar reduction experiments at low pressures ($P_{CO} < 10$ Pa), pure Mg particles were obtained at temperatures of 730-870 K on the deposit sites. Further, under low pressures, the magnesium vapor is in hyper-saturated state granting its easy nucleation and condensation at cooled condensation zones with temperatures lower than 830 K.[27,28] Furthermore, increasing the C/MgO molar ratio promotes the reverse reaction.[29,30]

Since 1996, it was proved that coconut charcoal is more reactive than graphite due to its higher surface area (1050 $m^2 g^{-1}$) allowing a higher contact area with MgO particles.[31] Also, they confirmed that the reaction rate declines as the carbon particle size and the carbon content decrease suggesting that the rate controlling step occurs on the carbon surface. Later on, the kinetics of magnesia reduction showed that charcoal is better than graphite at T < 1850 K, while above this temperature the carbon type does not affect the reaction rate as the gas diffusion becomes the rate-determining step due to the loss of the C/MgO contact.[32] The same conclusion was obtained during the solar-driven vacuum-assisted reduction of MgO using activated charcoal (AC, 732 $m^2 g^{-1}$) and carbon black (CB, 44 $m^2 g^{-1}$). It was found that the reaction rate is faster using AC than CB at first, and then it follows the same trend and this behavior was attributed to the two-step reaction where at low temperature the rate is favored by the C/MgO contact (phase boundary reaction), while at high temperature the rate is determined by the gas-solid reaction independently from the carbon type.[33] Those conclusions were confirmed by solar experiments, performed using biochar reductant at 1000 Pa, showing a good correlation for the MgO reduction kinetics with the phase boundary and nucleation reactions during the first stage of the reaction (20 s) with an activation energy of 210 and 220 kJ mol^{-1} respectively. Whereas, during this period, the diffusion reaction presents a poor correlation with an activation energy of 440 kJ mol^{-1}. After this period, several mechanisms are involved in the magnesia reduction as the three possible kinetics correlates well the experimental results. Thus, under vacuum conditions, the solid phase-boundary reaction will dominate until the C/MgO contact is reduced and at this stage, the gas diffusion becomes the rate-limiting step of the reaction.[34] Those findings become less important at high pressures (10 kPa) where various carbon types (petroleum coke, charcoal, and carbon black) showed similar reactivity, despite that charcoal has a higher surface area, as the solid-gas

MgO/CO reaction dominates independently from the C/MgO contact and the carbon properties.[35]

Therefore, those studies motivate us to investigate the effect of the charcoal properties (source, pyrolysis conditions, C-content…) on the magnesia solar carbothermal reduction under low pressures, aiming to improve the magnesium production. Moreover, the positive effect of the mechanical milling of carbon particles with magnesia powders and the catalytic effect of bentonite binder are highlighted proving that high yields of pure Mg powders are obtained by progressively increasing the reaction temperature. Hence, this study aims to efficiently regenerate the metal fuels using concentrated solar power (CSP) as a renewable energy source under the ANR STELLAR project in collaboration with STELLANTIS group.

2. Materials and methods

In this section, we present the procedure for the solar carbothermal reduction of magnesia under low pressures using various carbon reductants and we define the parameters to compare the performance of those experiments.

2.1 Experimental set-up

A 1.5 kW solar furnace, consisting of a heliostat with a solar tracking system that reflects the solar radiation to a parabolic mirror, was used to concentrate the solar power up to 15000 suns for the carbothermal reduction of magnesia. The solar experiments were performed in the Sol@rmet reactor,[36] shown in **Figure 2**, at low pressures (around 850 Pa) when the direct normal irradiation (DNI) was of 950-1020 W m^{-2}. The DNI variation along the reaction was less than 20 W m^{-2}. The vacuum was created using a dry primary pump (Edwards nXDS15i) with a maximum pumping rate of 15 m^3 h^{-1} and the pressure was adjusted by controlling the argon (carrier gas) flow rate. Argon was injected from the upper part of the reactor at 1 L

min^{-1} and from the bottom part of the reactor at 3.5 L min^{-1} thus creating a good swirl circulation to purge the produced powders.[37] The produced powders were collected on a porous stainless-steel filter (0.2 μm, 98%) placed on the entry of the pumping tube. However, a small quantity of products was condensed on the reactor walls. The temperature of the C/MgO pellet surface is measured using an optical monochromatic pyrometer (Heitronics K15.42 II, 5 μm) supposing the normal spectral emissivity of the pellet of 0.95. The pyrometer calibration was carried out on a black body up to 2000 K, giving a temperature accuracy of ± 50 K. Moreover, argon is injected from the upper tube to clean the CaF_2 window (*see* ***Figure 2***), which allows a good temperature measurement. Further, one must consider that the real spectral normal emissivity of the pellet can be affected by the C/MgO pellet properties (carbon type and fixed-carbon content). Nevertheless, if the spectral normal emissivity can be as low as 0.85, the effect on the real temperature will vary from 50 up to 150 K for respectively temperatures of 1500 and 2500 K. Unfortunately, we cannot measure the spectral normal emissivity for all the pellets thus, when comparing the temperature measured during the different experiments, using various carbon reducing agents, one must pay attention that all the temperatures are given supposing a 0.95 spectral normal emissivity for the C/MgO pellet, that we consider as a valid assumption. Previous modelling results proved that the expected temperature is around 100-200 K lower than the measured temperature.[34] However, those results are not certain as the numerical model contains several assumptions. We define T_i as the initial temperature when the reaction begins (first appearance of the CO peak) and T_m as the maximal temperature attained during the reduction.

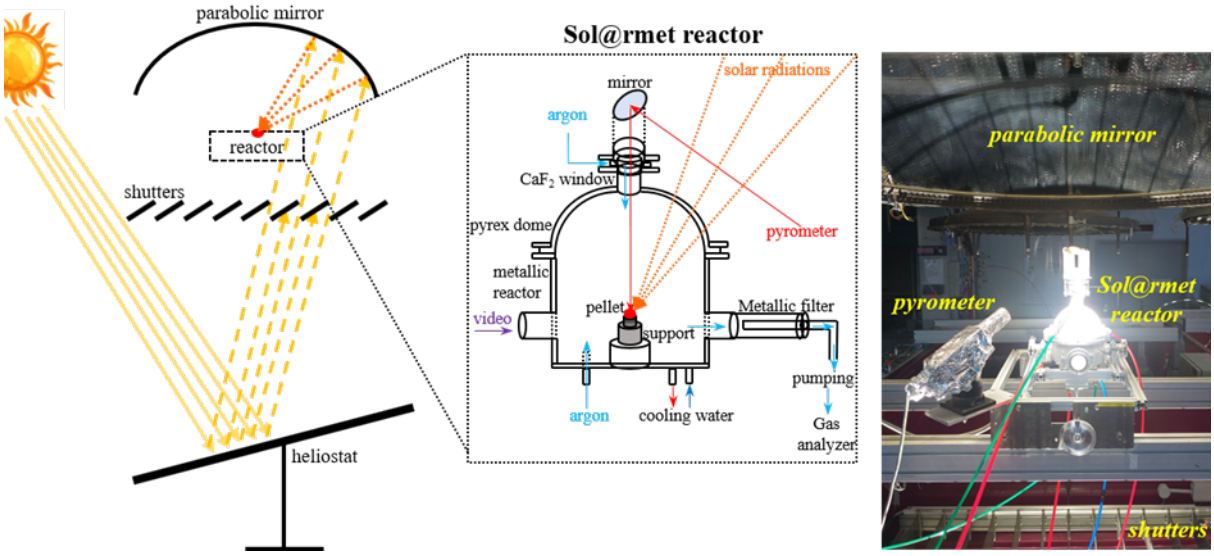

Figure 2. *Experimental set-up and photo of the concentrating solar system and the Sol@rmet reactor.*

2.2 Chemicals

Pure magnesia (Sigma-Aldrich, > 99%, Ø < 44 µm) and carbon reducing agent were mechanically milled with a C/MgO molar ratio of 1.25 using Fritsch Pulverisette 4 mill. Cylindrical pellets (Ø = 8 mm, thickness = 2-3 mm) are formed by dry pressing the milled powders at one ton. Bentonite (Sigma-Aldrich) and starch (Avedex 36 LAC 14, Avebe) binders were used to improve the mechanical stability of the C/MgO pellets. For some carbons, pellets could not be formed following the dry pressing method (DP) so C/MgO powders were wet-impregnated (WI) with the binders, molded by hand then dried at 413 K overnight. The following carbons are used and compared:

- Purchased carbons: graphite (Timcal HSAG300), carbon black (Cabot Carbone), Carbon Terra charcoal (birch wood pyrolysis at 770 K for 4 h), activated charcoal Norit® CA1 (Sigma-Aldrich, from wood), activated charcoal Norit® SX2 (Sigma-Aldrich, from peat), vegetable charcoal (France-herboristerie, Carbo liyni), coconut shells activated charcoal (Onatera), beech and birch activated charcoal (Onatera), bamboo charcoal (AliExpress).
- Chimney charcoal (charcoal collected from the residues of the house chimney).

- Charcoals synthesized by pyrolysis in a tubular furnace at 1083 K for 30 min under 10 $L \cdot h^{-1}$ of helium (at 2 K min^{-1}) of various biomass: Saccharose (VWR), coconut sugar, cornstarch, psyllium blond ispaghula, okara (dried at 413 K overnight or not), chaga mushroom, arrowroot starch.
- Charcoals synthesized by pyrolysis at 1083 K for 30 min (at 10 K min^{-1}) of various biomass: α-cellulose (Sigma-Aldrich), fucus vesiculosus, okara (dried at 413 K overnight), psyllium, panela cane sugar.
- Charcoal synthesized by pyrolysis at 783 K for 30 min (at 2 K min^{-1}) of psyllium.
- "Cellulose leav-charcoal" synthesized by pyrolysis at 1083 K for 30 min (at 10 K min^{-1}) of α-cellulose following the leavening method using bicarbonates as leaven agent (bicarbonates/cellulose mass ratio of 4). The produced charcoal is washed by an HCl solution (VWR, 37%, 1:1) and dried at 383 K overnight.

2.3 Carbon characterization

The chemical properties of the carbon reducing agents are determined through thermogravimetric analysis using TGA Q500 (TA instruments). Samples are heated at 10 K min^{-1} under nitrogen flow (0.1 L min^{-1}) from room temperature to 378 K to remove the humidity, then to 1173 K to remove the volatiles. Under those conditions, the mass loss of the sample corresponds to the water and volatiles contents respectively. At this temperature (1173 K), the gas is changed to air (0.1 L min^{-1}) and stabilized for one hour granting the combustion of the carbon atoms. The mass loss during this stage corresponds to the fixed carbon content (C-content). Finally, samples are cooled slowly and the remaining mass corresponds to the ash content.

The textural and structural properties of the carbon reducing agents are determined through N_2 adsorption/desorption isotherms at different relative pressures P/P_0 using ASAP

2020 (Micromeritics) after being degassed at 423 K. The surface area, pore volume and pore size distribution of those samples are calculated by BJH, BET and/or DFT methods.

2.4 Set of experiments

Two sets of magnesia vacuum-assisted carbothermal reduction solar experiments are performed by gradually opening the shutter placed between the heliostat and the parabolic mirror to increase the reaction temperature:

- "partial-reduction": the shutter is opened progressively up to 60% over 18 min. These tests are dedicated to compare the performance of various carbon reducing agents by computing the maximal temperature attained (T_m) and the Mg yield under the same solar heating procedure,
- "total-reduction": the shutter is opened gradually by 10% each two minutes, until fully opened and the reaction lasts for 22 min. In this case, the best carbon reducing agent is chosen and the experiments aim to probe the catalytic-like role of bentonite binder and to increase the magnesium yield.

2.5 Performance criteria

The produced powders, collected on the filter and the reactor walls, were analysed by X-ray diffraction (PANanalytical X'Pert Pro) and the approximate percentages of Mg and MgO are quantified using Highscore Plus software (comparing to International Centre for Diffraction Data ICDD files using reference intensity ratio technique). Whereas, the gaseous products (CO and CO_2) were analysed with time during the reaction using the Xstream X2GP infrared gas analyzer (Emerson). The morphology and size of the powders are determined by granulometric analysis (Malvern Mastersizer 3000) and Scanning Electron Microscopy (SEM) images.

The performance of the magnesia reduction is computed by calculating the magnesium metallic yield (y_{Mg}) according to *equation (1)*, where m_{Mgmax} is the maximum quantity of Mg that can be produced based on the initial magnesia molar quantity, $\%Mg_{filter}$ and $\%Mg_{reactor}$ are the percentages of Mg purity of the powders collected on the filter and the reactor walls respectively. The yield calculation uncertainty for all the measurements is mainly dependent on the semi-quantitative XRD measurements (% Mg) and on the ability to collect all the produced powders in the reactor. Previous corrected Rietveld refinement XRD calculations proved that the semi-quantitative XRD measurements give a variability of less than 3% for nearly-pure Mg powders (more than 90% Mg). Further the remaining non-collected powders in the reactor present less than 3% of the total collected quantity (less than 1 mg). Therefore, an uncertainty of ± 3% is considered for the yield calculation for all the experiments.

$$y_{Mg}\,(\%) = 100\,\frac{m_{filter}\ \ \%Mg_{filter} + m_{reactor}\ \ \%Mg_{reactor}}{m_{Mgmax}} \qquad (equation\ 1)$$

3. Comparison of various carbon reducing agents

In this section, we compare the solar carbothermal reduction of magnesia under low vacuum conditions using various carbon reducing agents by discussing the effect of their source, production and properties on the magnesium yield. Despite the previous works in this field, none of them, to our best knowledge, investigated the effect of the charcoal properties and how controlling the pyrolysis conditions (and biomass source) affects the reduction yield. Moreover, a carbon reducing agent suitable for the CTR in a tube furnace or in a solar simulator is not necessarily appropriate to use for the CTR using real concentrated solar conditions. For example, the temperature cannot be increased rapidly using a tube furnace as when using CSP (up to 1000 K s^{-1}) and the spectrum generated using a solar simulator

(Xenon lamps) is different from the one of the sun when using CSP. Furthermore, the C/MgO pellet properties (solar absorptivity, C/MgO contact, MgO sintering…) are affected by the carbon reducing agent and change along the reaction (damage and consumption of the pellet). These parameters impact the maximal temperature attained (T_m), the reaction mechanisms and thus the reduction yield. Unfortunately, the solar absorptivity is difficult to measure at the operating temperatures and the various mechanisms (sintering, contact) are hard to be examined as the reaction proceeds.

3.1 Effect of the mechanically milling of the C/MgO powders

The effect of the mechanical milling of the C/MgO powders on the magnesia reduction was previously confirmed as it decreases the particle size and increases the C/MgO contact.[37] In this study, we affirmed this effect by comparing the "partial-reduction" of magnesia using bamboo charcoal when the particles are milled mechanically or manually with 5% starch. As a result, a higher magnesium yield of 64.2% is reached when the C/MgO particles are mechanically milled compared to 51.0% when milled manually, confirming the previous conclusions. The produced powders were mainly collected on the metallic filter at the exit tube, with some small part deposited on the reactor walls. Those powders collected on the filter were highly pure with around 95% Mg, as shown in **Figure 3**, while those deposited on the walls were less pure (around 75% Mg). Operating under low vacuum (840 Pa) and for low C/MgO molar ratio (of 1.25) limited the re-oxidation of the produced powders (through the reverse CO/Mg reaction) collected on the metallic filter where the temperature is close to room temperature. However, the small part collected on the cooled metallic parts of the reactor walls, having temperatures up to 500 K,[37] suffered from the reverse re-oxidation (up to 25%). The remaining part of the C/MgO pellet consists of unreacted magnesia with some small quantities of $Mg(CO_3)$ and graphitized carbon.

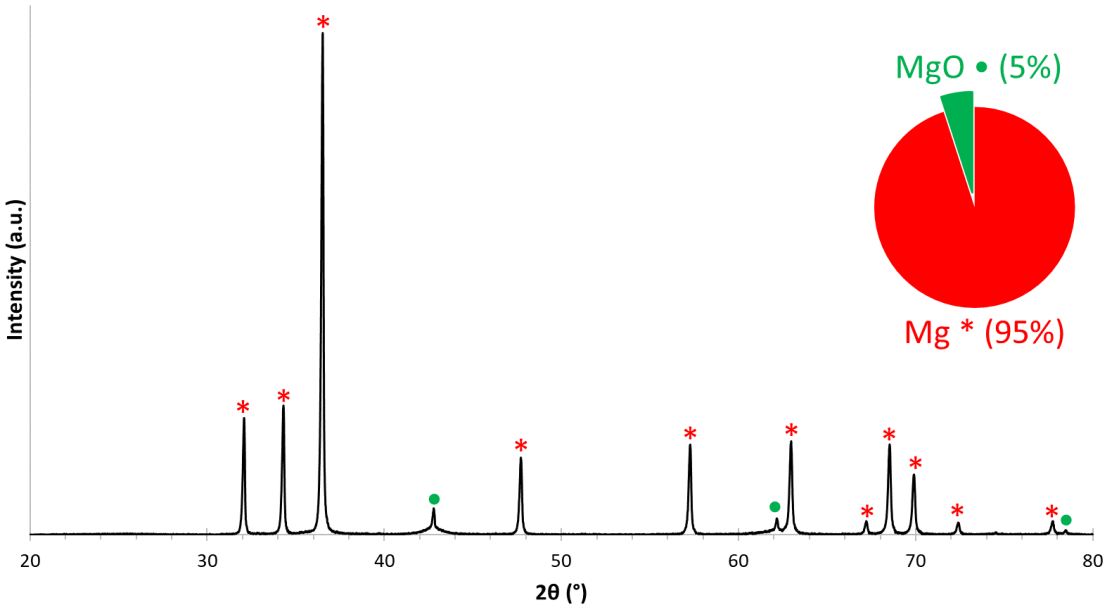

Figure 3. *XRD pattern of the powder collected on the filter after the solar carbothermal reduction of magnesia, under low pressure, using bamboo charcoal.*

3.2 Effect of the C/MgO pelletization method

As mentioned in section 2.2, some of the carbon could not form a mechanically stable pellet with magnesia by dry pressing (DP), even using starch binder. In this case, they are wet impregnated (WI) with the starch to improve the binding effect and thus the formation of the C/MgO pellet. **Table 1** presents the results of the "partial-reduction" of C/MgO pellets formed through DP or WI methods using various carbon reducing agents. The pelletization method affects the Mg yield as when comparing tests A1 and A2 using Carbon Terra charcoal, the Mg yield decreases by around 10% when powders are wet-impregnated. This can be attributed to the hydration of magnesia and the formation of $Mg(OH)_2$ which accelerates the sintering effect.[38] The maximal temperature reached (T_m) during the reduction is 2260 K when the C/MgO pellet is formed through DP, about 200 K higher than when formed through WI, despite that the initial temperature was similar (T_i around 1250 K) and that the DNI was lower during experiment A1 (950 compared to 1030 W m^{-2}). This confirms

that, under similar solar-heating procedure, the maximal temperature reached (T_m) and the Mg yield are dependent on the C/MgO properties that change throughout the reaction rather than the DNI. Remarkably, when comparing the magnesium production using Carbon Terra or Norit® CA1 charcoals (WI method), we can state that the reduction is affected mainly by the fixed C-content and not by the surface area of the charcoal as that of Carbon Terra is much lower than that of Norit® CA1 (150 compared to 1315 $m^2 g^{-1}$) giving however a higher Mg yield of 55.1% at similar DNI (difference < 30 W m^{-2}). When comparing experiments A4 and A5, we demonstrated that using charcoal Norit® SX2 (88% C-content) allows reaching a maximal temperature of reduction T_m of 2070 K higher than when using charcoal Norit® CA1 (81% C-content, T_m = 1840 K) and thus higher reduction yield. In fact, Norit® SX2 charcoal is obtained from peat biomass, which is known to give superior quality charcoal.[39]

Figure 4 shows the temperature profile and the gaseous emissions (CO and CO_2) during the solar vacuum-assisted carbothermal reduction of magnesia using Carbon Terra charcoal or carbon black as reducing agents. Despite the higher temperature reached (test A6, 2285 K at 950 W m^{-2}) using carbon black compared to Carbon Terra charcoal (test A2, 2060 K at 1030 W m^{-2}), the latter gives a better Mg yield due to its amorphous structure compared to the crystalline structure of carbon black.[40] Furthermore, we proved that none of the pellets formed through WI using different carbon reducing agents outperformed the pellet formed through DP using Carbon Terra charcoal. Thus, the dry pressing method is admitted for the following comparison of various charcoals.

Table 1. *Comparison of the reduction performance depending on the carbon reducing agent and the pelletization method (DP vs WI).*

Test	Reducing agent	Pelletization method	C-content (%)	T_i - T_{max} (K)	Mg yield (%)	DNI (W m^{-2})
A1	Carbon Terra charcoal	DP	94	1250 - 2260	63.3	950
A2	Carbon Terra charcoal	WI	94	1230 - 2060	55.1	1030
A3	Charcoal Norit® CA1	WI	81	-	30.1	1000
A4	Charcoal Norit® CA1	WI	81	1300 - 1840	29.8	990
A5	Charcoal Norit® SX2	WI	88	1300 - 2070	60.1	1020
A6	Carbon black	WI	98	1180 - 2285	29.9	950

DP and WI refer to "dry pressing" and "wet impregnation" respectively.

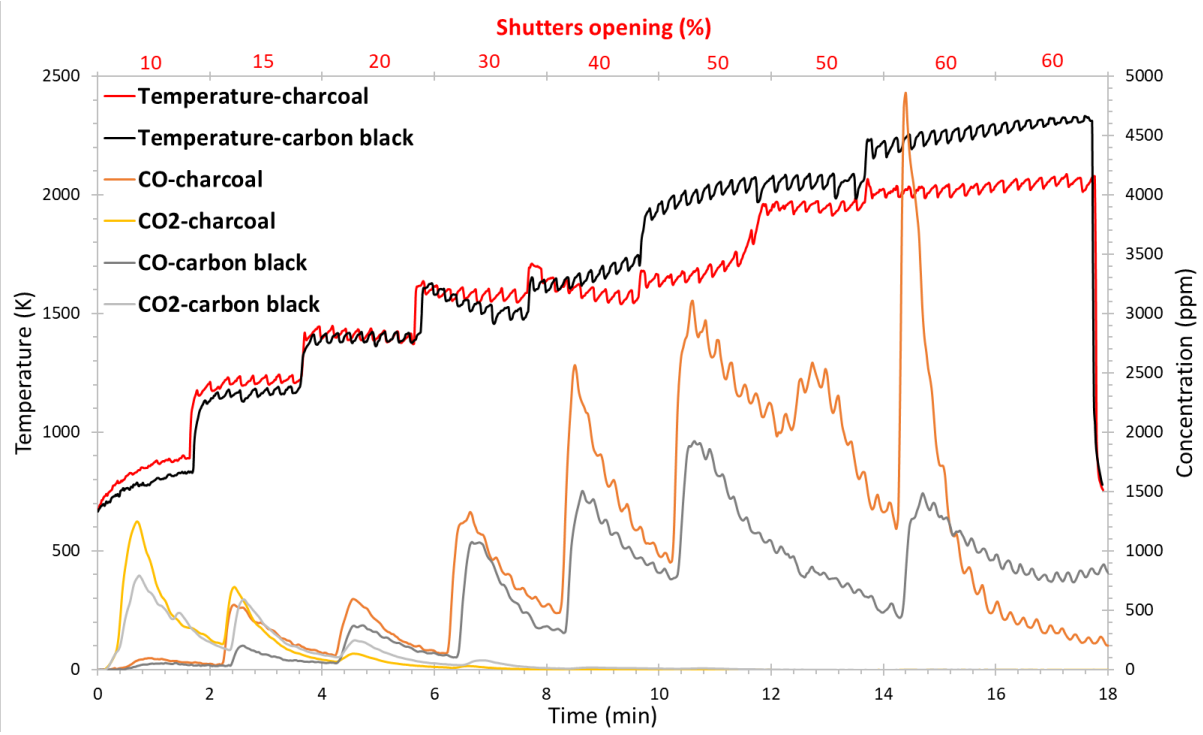

Figure 4. *Temperature and gaseous emissions (CO and CO_2) variation during the solar vacuum-assisted reduction of magnesia using Carbon Terra charcoal or carbon black as reducing agent.*

3.3 Effect of the biomass drying

In this section, we investigate the effect of drying the biomass before the pyrolysis on the fixed C-content and consequently the reduction yield. Okara biomass consists of a pulp of

insoluble parts of the soybean remaining during the production of soy milk. The fixed C-content of the charcoal produced from the pyrolysis of okara increases from 63 to 72% when okara is dried overnight at 413 K. This allows reaching higher temperature during the magnesia reduction (same solar-heating procedure) attaining a T_m of 1830 K instead of 1710 K despite that the DNI was slightly lower (970 W m^{-2} for dried okara compared to 1020 W m^{-2} for non-dried okara). Thus, a slightly higher Mg yield of around 45% instead of 39% was obtained. This can be attributed to that increasing the C-content improves the solar absorptivity of the C/MgO pellet, reduces the magnesia sintering and maintains the C/MgO contact all along the reaction.

3.4 Effect of the carbon type and biomass source

To determine the impact of the reducing agent, we compared in **Table 2** the performance of the magnesia solar reduction experiments using various commercial carbons. We proved that the reaction is mainly affected by the carbon type and the fixed C-content. For example, the Carbon Terra charcoal (experiment B1) allows reaching a higher Mg yield than graphite M-291 despite that they have the same fixed C-content and that graphite has a higher surface area. The properties of the C/MgO pellet are dependent on the carbon reducing agent and its interaction with the magnesia particles throughout the reaction. Using Carbon Terra charcoal allows to attain a higher maximal temperature T_m of 2260 K compared to 2090 K when using graphite, despite that the DNI was lower (950 compared to 1020 W m^{-2}) and that both reactions started at similar temperatures (T_i = 1200 - 1250 K). This can be attributed to the amorphous structure of charcoal that is more active than the crystalline graphite structure.[40] Comparing experiments B1 and B3 assured that the choice of the charcoal is unconstrained by its surface area as both Carbon Terra and coconut shells activated charcoals showed similar yields despite the large difference between their BET surface values (150 compared to

1200 m^2 g^{-1}). Further, despite the higher DNI during test B3, a lower temperature of 1980 K (at 980 W m^{-2}) is attained compared to 2260 K during test B1 (950 W m^{-2}), but this did not affect the yield. Meaning that the maximal attained temperature is not the only parameter that affects the yield, rather one must consider the various phenomena that occur along the reduction such as the C/MgO pellet structural damage, the MgO sintering and the C/MgO contact. The pore volume, at P/P_0 of 0.99, of the Carbon Terra charcoal is around 15% that of coconut shells activated charcoal (0.08 compared to 0.53 cm^3 g^{-1}). However, this difference did not affect the reduction yield as, under our operating experimental conditions, the phase boundary reaction dominates the solid-gas (MgO-CO) reaction that can be impacted by the carbon porosity. The pore size distribution is similar for both charcoals with an average BET pore diameter of 21.4 and 17.6 Å for Carbon Terra and coconut shells charcoals respectively. However, according to DFT measurements, all of the pores of coconut shells charcoal are macro-sized while Carbon Terra charcoal presents additionally to macropores some micropores (0.006 cm^3 g^{-1} for $d < 8$ Å). These diameters are very small and do not affect the reaction, rather the reaction is affected by the external surface of the carbon particles and their direct contact with large MgO particles (*see* ***Figure 7***).

Table 2. *Comparison of the reduction performance depending on the carbon reducing agent.*

Test	Reducing agent	BET surface ($m^2 g^{-1}$)	C-content (%)	T_i - T_{max} (K)	Mg yield (%)	DNI ($W m^{-2}$)
B1	Carbon Terra charcoal	150	94	1250 - 2260	63.3	950
B2	Chimney charcoal	< 1	43	1220 - 1640	30.3	1010
B3	Coconut shells activated charcoal	1200	90	1300 - 1980	65.9	980
B4	Beech and birch activated charcoal	-	86	1300 - 1980	65.3	1000
B5	Vegetable charcoal	1210	78	1290 - 2150	59.6	960
B6	Bamboo charcoal	-	93	1280 - 2020	64.2	960
B7	Graphite M-291	255	94	1200 - 2090	37.6	1020

As conclusion, we demonstrated that, using wood-based charcoals, a minimum C-content of 80% is required and sufficient to perform a good reduction (Mg yield around 65%) as the Mg yield decreases slightly to 60% during experiment B5 (vegetable charcoal with 78% C) and to 30% during experiment B2 (chimney charcoal with 43% C). The product powders collected on the filter after experiment B1 consist of agglomerates of sub-micron Mg crystals and particles as shown in **Figure 5 (left)**. The granulometry analysis proved those observations with a D_{10}, D_{50} and D_{90} diameters of around 3, 23 and 77 µm respectively. In fact, around the third of the produced powders are smaller than 10 µm, the two-third are smaller than 30 µm and 95% are smaller than 100 µm. **Figure 5 (right)** shows a SEM image of the residual of the C/MgO pellet remaining after the end of experiment B1. It consists mainly of large sintered agglomerates of magnesia (as determined by XRD) with a D_{90} diameter higher than 200 µm.

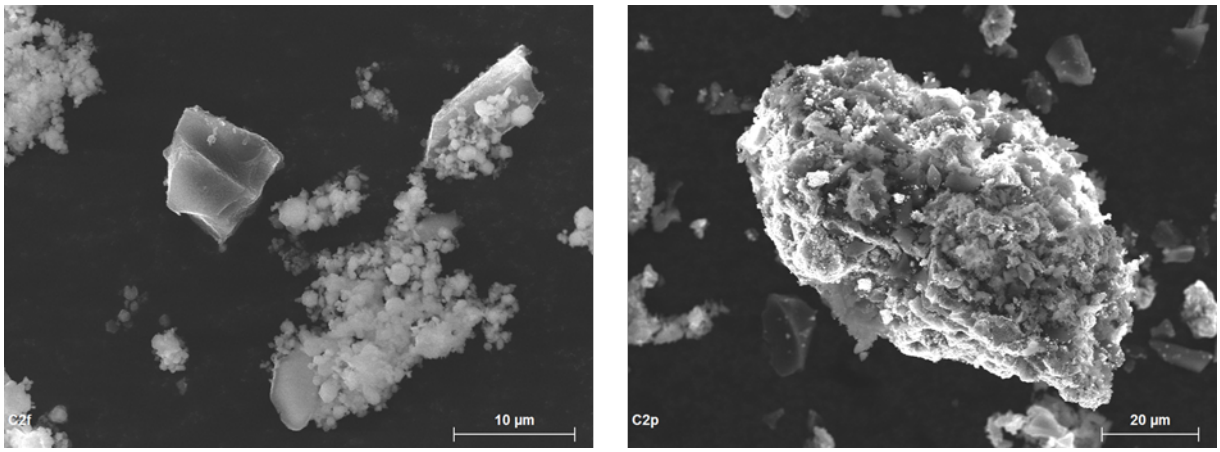

Figure 5. *SEM images of the produced Mg powders collected on the filter (left) and of the remains of the C/MgO pellet (right) after experiment B1.*

When comparing the solar reduction experiments using laboratory-synthesized charcoals using various non-wood biomass sources (**Table 3**), we have shown that not only the fixed C-content is the key-parameter, but also the biomass source. For example, sugar-based charcoals (tests C1 and C2) gave a Mg yield not exceeding 40% despite having a C-content higher than 80%. Nevertheless, charcoals having a C-content lower than 80% (experiments C3 and C7 using okara dried and chaga mushroom respectively) yielded less than 50% magnesium. Whereas, a high Mg yield (around 65%) is obtained using cornstarch, arrowroot starch or psyllium charcoals having a C-content > 85%. Thus, we conclude that a minimum fixed C-content of 80% is needed but not necessarily sufficient to perform a good reduction, rather the biomass source is crucial parameter to consider where wood-based, starch-based and psyllium charcoals show a superior performance as reducing agents. Furthermore, when comparing experiments C1 and C6, results proved that the Mg yield depends on the biomass source (psyllium vs. saccharose) despite that both charcoals have similar C content and BET surface area (117 vs. 108 $m^2 g^{-1}$). Moreover, laboratory-synthesized psyllium charcoal gives around 64% Mg yield, higher than that obtained using purchased vegetable charcoal (experiment B5, 60% Mg yield) despite having a BET surface area around ten times lower (117 vs. 1210 $m^2 g^{-1}$).

Table 3. *Comparison of the reduction performance depending on the biomass source.*

Test	Biomass source	BET surface (m^2 g^{-1})	C-content (%)	Ti - T_{max} (K)	Mg yield (%)	DNI (W m^{-2})
C1	Saccharose	108	86	1200 - 2020	37.9	990
C2	Coconut sugar	13	81	1280 - 2090	40.0	1000
C3	Okara dried	-	72	1300 - 1830	44.9	970
C4	Cornstarch	209	89	1300 - 2000	65.2	990
C5	Arrowroot starch	184	88	1350 - 2100	67.7	960
C6	Psyllium	117	85	1350 - 2050	63.6	970
C7	Chaga mushroom	34	56	1240 - 1670	48.9	1000

The pyrolysis of those biomass is performed at 1083 K for 30 min (at 2 K min^{-1}).

3.5 Effect of the pyrolysis heating rate and temperature

The effect of the pyrolysis conditions on the quality of charcoal as a reducing agent were studied and optimized according to its CO_2 reactivity.[41] According to some results, the charcoal reactivity is rather dependent from the wood source and negligibly dependent form the pyrolysis conditions.[42] Herein, we investigated the effect of the pyrolysis conditions on the quality of charcoal as a reducing agent during the reduction of magnesia using concentrated solar energy. We proved that the highest Mg yield of 63.6% and reduction temperature of 2050 K were attained when operating at higher pyrolysis temperature (1083 K) and low pyrolysis heating rate (2 K min^{-1}). In this case, a high fixed C-content of 85% is reached allowing a better C/MgO contact and preventing the magnesia sintering. In comparison, a Mg yield of 26.0% and a reduction temperature of 1560 K were obtained when a pyrolysis heating rate of 10 K min^{-1} (at 1083 K) is admitted. Whereas using a pyrolysis temperature of 783 K (at 2 K min^{-1}), a maximum reduction temperature of 1700 K is reached

giving a Mg yield of 33.6%. Those results are attributed to the lower C-content of 76 or 78% obtained at 10 K min^{-1} (at 1083 K) or 783 K (at 2 K min^{-1}) respectively. Similarly, when okara dried biomass is used, a higher Mg yield is obtained when admitting a lower pyrolysis heating rate of 2 K min^{-1} instead of 10 K min^{-1} (44.9% compared to 30.7%). **Figure 6** compares the variation with time of the temperature and the cumulative CO concentration during the magnesia solar reduction using psyllium charcoal (synthesized at two pyrolysis heating rates) or okara dried charcoal (pyrolysis at 2 K min^{-1}). The temperature and CO concentration profiles are consistent with the Mg yield results confirming the effect of the pyrolysis conditions and biomass on the charcoal reductant grade.

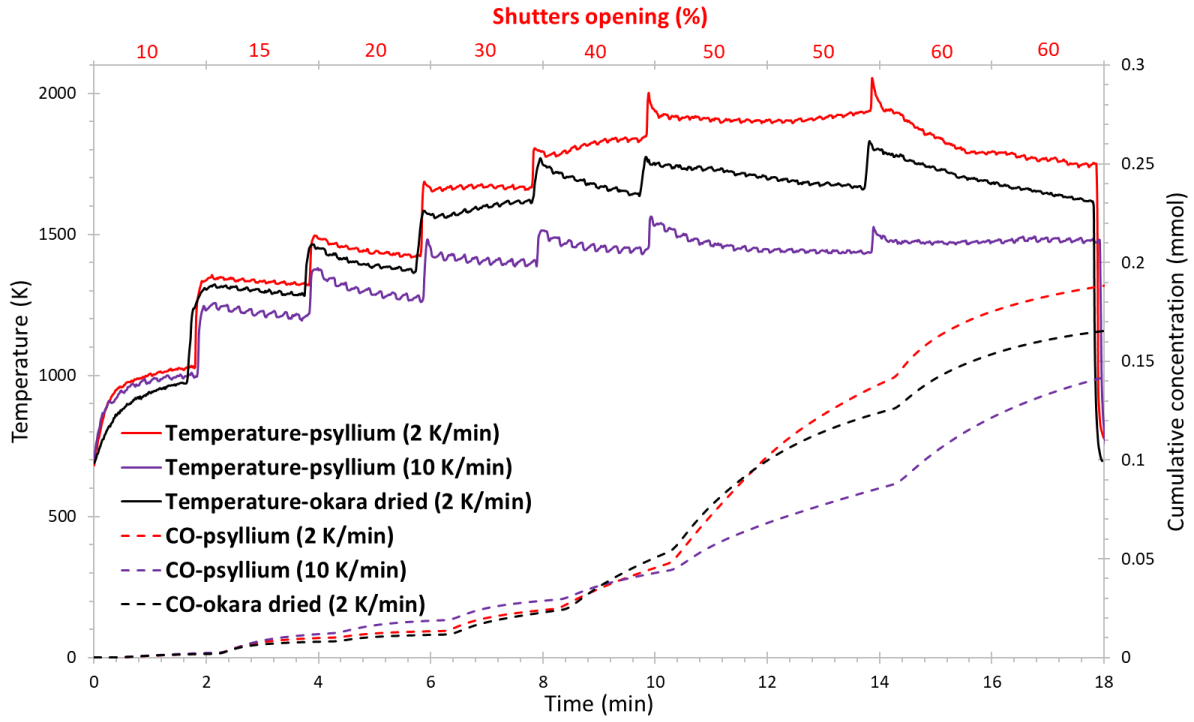

Figure 6. *Temperature and CO cumulative concentration profiles during the solar vacuum-assisted reduction of magnesia using psyllium (at different pyrolysis heating rates) or okara dried charcoals.*

3.6 Effect of the pyrolysis leavening method

The pyrolysis following the leavening method is inspired by bread leavening to obtain hierarchically porous carbon.[43] The performance of cellulose charcoal and cellulose leav-

charcoal as reducing agents for magnesia reduction is interpreted proving that the leavening method is disadvantageous. Despite the high surface area (1000 compared to 233 $m^2 g^{-1}$) and pore volume (0.106 compared to 0.564 $cm^3 g^{-1}$) achieved following the leavening method, the magnesium yield obtained using cellulose leav-charcoal is lower than that obtained using cellulose charcoal (37% compared to 58%) as the fixed C-content is lower (59% compared to 88%). Further, under similar DNI, the maximal temperature attained T_m could not exceed 1730 K (at 960 W m^{-2}) using the cellulose leav-charcoal (having lower C-content) compared to 2070 K (at 1010 W m^{-2}) when using cellulose charcoal. As proved before, the small DNI difference (50 W m^{-2}) does not affect the results, rather the properties and mainly the C-content is the key parameter for the reducing agent. Contrarily, the high surface area (resulting from the high pore volume) does not necessarily affect the magnesium production. As explained previously (section 3.4), in our operating conditions, the phase boundary C/MgO reaction dominates the gas-solid reaction. The former depends mainly on the C/MgO contact surface and not necessarily on the carbon surface area (affected by the porosity), contrarily to the latter where an easy circulation of CO in the carbon porosity is attractive.

4. Efficient magnesium production using solar power

In the following section, the solar experiments were performed to increase the production yield of pure magnesium fuel powders through the carbothermal reduction of magnesia using Carbon Terra charcoal and by gradually increasing the temperature until the shutters are fully opened over 22 min (*see section 2.4*). The choice of Carbon Terra charcoal is based on the results obtained in the previous section as it has a high fixed C-content of 94% resulting high reduction temperatures of 2260 K and high Mg yield of around 63% when performing "partial reduction" and using 5% starch as binder. However, the pelletization of C/MgO powders into a mechanically-stable pellet is better accomplished by using a 5% starch – 5%

bentonite.[44] Moreover, the mechanical milling of the C/MgO powders with the starch-bentonite binder prevents the existence of agglomerates, decreases the particle size and increases the C/MgO contact as shown in **Figure 7**, thus improving the reduction yield.[37] Inspired by a previous study confirming the catalytic-like role of calcium fluoride,[45] **Table 4** compares the magnesium yield and purity during the solar reduction experiments of magnesia using C/MgO pellets with 5% starch or 5% starch - 5% bentonite binders.

Table 4. *Catalytic-like effect of bentonite binder on the Mg production yield during the solar carbothermal reduction of magnesia.*

Test	binder	Ti - T_{max} (K)	DNI (W m^{-2})	$m_{reactor}$ (mg)	$Mg_{reactor}$ (%)	m_{filter} (mg)	Mg_{filter} (%)	Mg yield (%)
D1	5% starch	1250 - 2610	970	10.7	74*	79.6	93*	77.4
D2	5% starch**	1350 - 2550	970	12.0	74	55	93	74.8
D3	5% starch – 5% bentonite	1250 - 2490	960	21.4	58	77.3	96	87.4
D4	5% starch – 5% bentonite	1300 - 2490	1000	21.8	58*	85.7	96*	95.8
D5	5% starch – 5% bentonite**	1300 - 2470	1010	15.4	58	69.1	96	90.6
D6	5% starch – 5% bentonite	1270 - 2310[#]	990	18.8	58	80.2	96	88.3

**Values determined by semi-quantitative XRD measurements and admitted for other experiments.*
***C/MgO pellets of ~ 200 mg, for other experiments C/MgO pellet of ~ 250 Mg.*
[#] *Windy day which sometimes displaces the focus due to the movement of the heliostat mirror.*

The comparison of the magnesium production yields, obtained when 5% starch - 5% bentonite binder is used (experiments D3-D6) to those when 5% starch binder is used (experiments D1 and D2), proves the catalytic-like role of the bentonite binder. This role is attributed to the better integrity and contact between C/MgO particles as shown in **Figure 7** where no agglomerates are found using starch-bentonite binder, while some magnesia agglomerates (around 100 μm) are observed using starch binder. Those observations were

confirmed by granulometry analysis as the D_{90} particle size of the C/MgO powders decreases from 91 μm to 22 μm when starch-bentonite binder is used instead of using only starch. The magnesium yield is at minimum 10 % higher when using 5% starch - 5% bentonite binder instead of 5% starch binder (experiments D3 vs. D1). This difference attains around 20% with experiment D4 where the highest yield of about 96% of highly pure Mg powders (only 4% MgO) was reached using starch-bentonite binder. **Figure 8** shows that despite the higher reduction temperatures (up to 2600 K) observed during experiment D1 (using starch) compared to 2300 K during experiment D6 (using starch-bentonite), a higher CO production (0.207 vs. 0.163 mmol) and thus magnesium yield (88.3 vs. 77.4%) are obtained using bentonite binder that acts as a catalyst.

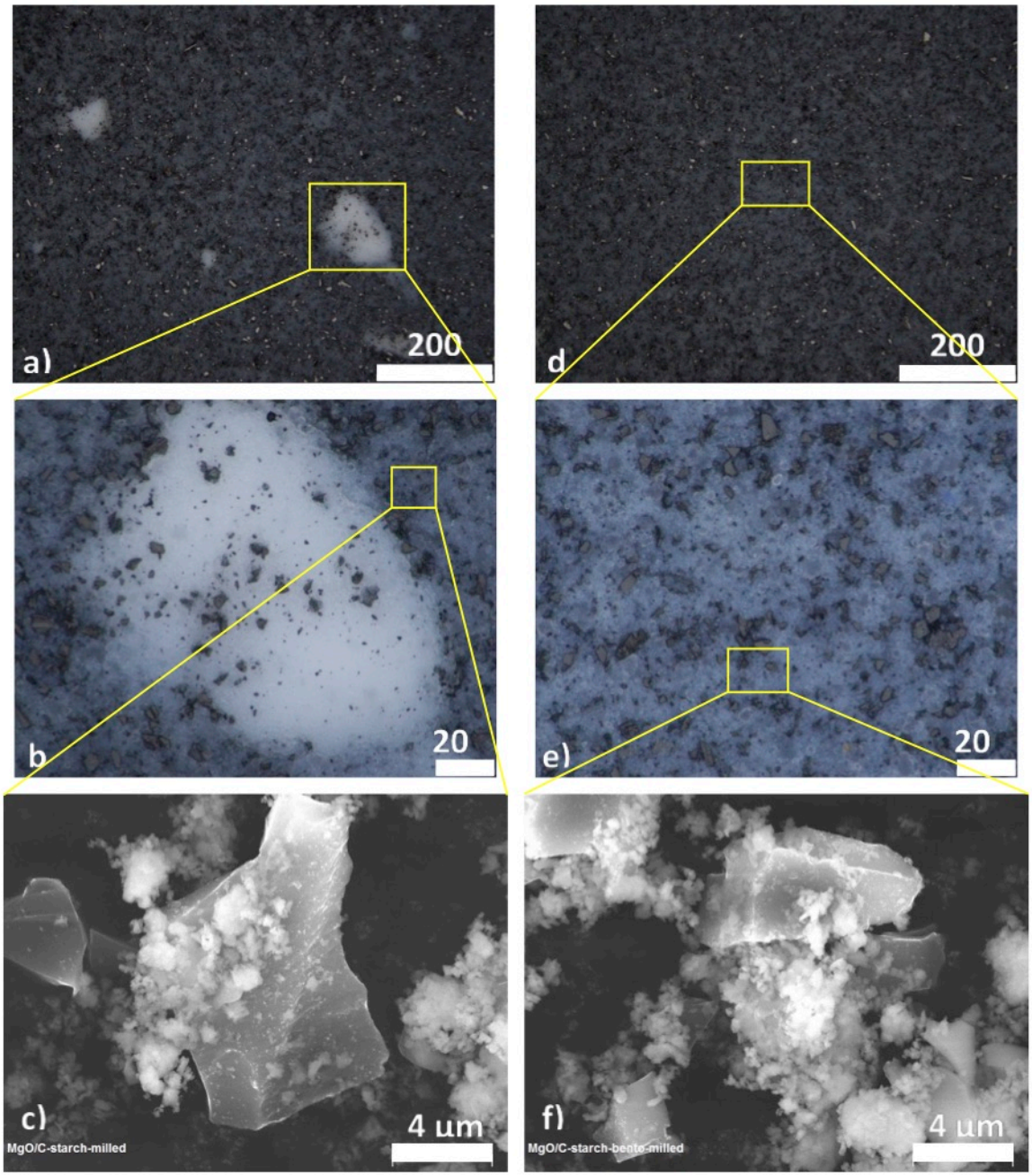

Figure 7. *Optical microscope and SEM images of the C/MgO powders with 5% starch (**a**, **b** and **c**) or with 5% starch – 5% bentonite (**d**, **e** and **f**) used during experiment D2 or D6 respectively.*

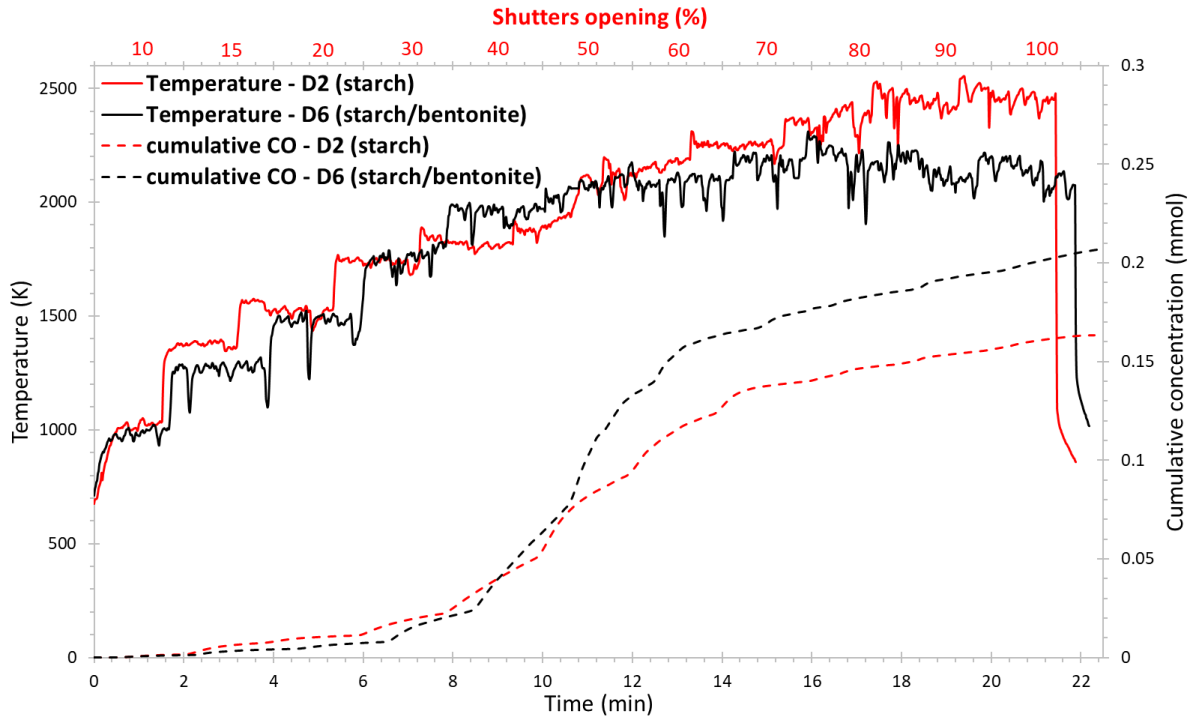

Figure 8. *Temperature and CO cumulative concentration profiles during the solar vacuum-assisted reduction of C/MgO pellet during experiment D2 (using starch) and D6 (using starch-bentonite).*

Figure 9 presents the SEM images of the powders produced from the magnesia solar reduction after experiment D4. Those powders consist of agglomerates of submicron magnesium crystals and particles with some native oxides (MgO) on the surface of the Mg crystals. The SEM images confirm the semi-quantitative XRD measurements that indicate a lower Mg purity as the surfaces of the Mg crystals are more oxidized (**Figure 9.d**). It is well clear that the powders collected on the filter are much smaller than those deposited on the reactor walls. Those observations were confirmed by granulometry analysis showing that the D90 particle size of the powders collected on the filter is around half that of powders deposited on the reactor walls (58 compared to 99 µm).

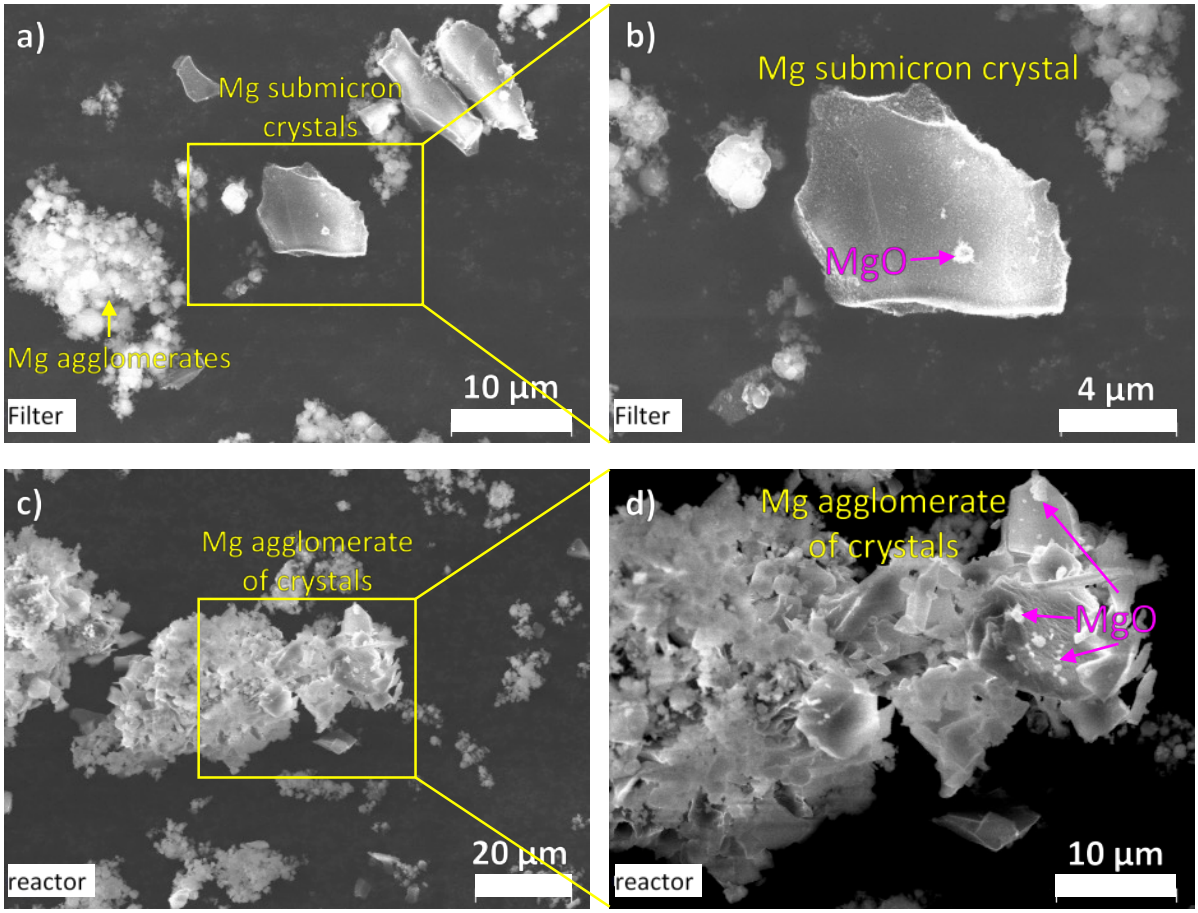

Figure 9. *SEM images of the produced powders collected on the filter (**a** and **b**) and deposited on the reactor walls (**c** and **d**) after magnesia solar carbo-reduction (experiment D4).*

5. Conclusions

This study discusses the vacuum-assisted carbothermal reduction of magnesia, using different carbon reducing agents, as a potential regeneration process of carbon-free metal fuels for transportation. The reduction experiments were performed in the Sol@rmet reactor using the concentrated solar energy provided by a 1.5 kW solar furnace at Odeillo. As the C/MgO phase boundary reaction is the dominant phase that controls the magnesia sintering and the reaction kinetics, the effect of the carbon properties (biomass source, pyrolysis conditions, fixed C-content, surface area) on the reduction yield was studied. Different charcoal reducing agents were synthesized through the pyrolysis of various biomass sources

under diverse pyrolysis conditions (drying, temperature, heating rate, leavening method). As a first result, we confirmed the importance of the mechanical milling of C/MgO powders as a method to increase the C/MgO contact and to decrease the particle size, thus improving the reduction yield. The comparison of various carbon reducing agents for the solar reduction experiments proved that charcoals are preferred over black carbon and graphite. Moreover, whatever is the charcoal used, the wet impregnation method is disadvantageous due to the partial magnesia hydration. Moreover, for wood-based, starch-based and cellulose-based (as psyllium) charcoals, a fixed carbon content higher than 80% is sufficient and necessary for a good reduction. Chimney, chaga mushroom and okara charcoals, having less than 80% C-content, showed a poor reducing agent quality. However, this C-content criterion is not sufficient when sugar-based charcoals (C-content > 80%) are used. The pyrolysis conditions can be optimized to achieve a good reduction yield for example for psyllium charcoal, a high pyrolysis temperature (1083 K) and a low pyrolysis heating rate (2 K min^{-1}) are preferred over 783 K and 10 K min^{-1} respectively. Finally, we have highlighted the catalytic-like effect of bentonite binder that allows achieving high yields (up to 96%) of highly pure Mg submicron agglomerates (96% purity).

Conflicts of Interest

There are no conflicts to declare

Acknowledgements

This study is funded under the STELLAR project by the French National Research Agency under contract ANR-18-CE05-0040-02. This work is supported by the French "Investments for the future" program managed by the French National Research Agency under contract ANR-10-EQPX-49-SOCRATE (Equipex SOCRATE).

References

1 M. Höök and X. Tang, *Energy Policy*, 2013, **52**, 797–809.
2 UN General Assembly, *Transforming our world: the 2030 Agenda for Sustainable Development*, 2015.
3 F. X. Dussud, I. Joassard, F. Wong, J. Duvernoy and R. Morel, UN Climate Change Conference, Paris, 2015.
4 J. M. Bergthorson, S. Goroshin, M. J. Soo, P. Julien, J. Palecka, D. L. Frost and D. J. Jarvis, *Appl. Energy*, 2015, **160**, 368–382.
5 E. I. Shkolnikov, A. Z. Zhuk and M. S. Vlaskin, *Renew. Sustain. Energy Rev.*, 2011, **15**, 4611–4623.
6 J. M. Bergthorson, *Prog. Energy Combust. Sci.*, 2018, **68**, 169–196.
7 P. Laboureur, R. Lomba, F. Halter, C. Chauveau and C. Dumand, https://hal.archives-ouvertes.fr/hal-01860128, Strasbourg, 2018.
8 R. Lomba, F. Halter, C. Chauveau, S. Bernard, P. Gillard, C. Mounaim-Rousselle, T. Tahtouh and O. Guezet, in *53rd AIAA Aerospace Sciences Meeting*, American Institute of Aeronautics and Astronautics, Kissimmee, Florida, 2015.
9 R. Lomba, S. Bernard, P. Gillard, C. Mounaïm-Rousselle, F. Halter, C. Chauveau, T. Tahtouh and O. Guézet, *Combust. Sci. Technol.*, 2016, **188**, 1857–1877.
10 P. Garra, G. Leyssens, O. Allgaier, C. Schönnenbeck, V. Tschamber, J.-F. Brilhac, T. Tahtouh, O. Guézet and S. Allano, *Appl. Energy*, 2017, **189**, 578–587.
11 D. Laraqui, O. Allgaier, C. Schönnenbeck, G. Leyssens, J.-F. Brilhac, R. Lomba, C. Dumand and O. Guézet, *Proc. Combust. Inst.*, 2019, **37**, 3175–3184.
12 D. Laraqui, G. Leyssens, C. Schonnenbeck, O. Allgaier, R. Lomba, C. Dumand and J.-F. Brilhac, *Appl. Energy*, 2020, **264**, 114691.
13 J. Murray, A. Steinfeld and E. Fletcher, *Energy*, 1995, **20**, 695–704.
14 P. G. Loutzenhiser, O. Tuerk and A. Steinfeld, *JOM*, 2010, **62**, 49–54.
15 E. Bilgen, M. Ducarroir, M. Foex, F. Sibieude and F. Trombe, *Int. J. Hydrog. Energy*, 1977, **2**, 251–257.
16 E. Alonso, C. Pérez-Rábago, J. González-Aguilar and M. Romero, *Energy Procedia*, 2014, **57**, 561–569.
17 I. Vishnevetsky and M. Epstein, *Sol. Energy*, 2015, **111**, 236–251.
18 Y. Lu, L. Zhu, C. Agrafiotis, J. Vieten, M. Roeb and C. Sattler, *Prog. Energy Combust. Sci.*, 2019, **75**, 100785.
19 A. Steinfeld, P. Kuhn and Y. Tamaura, *Energy Convers. Manag.*, 1996, **37**, 1327–1332.
20 B. Schaffner, W. Hoffelner, H. Sun and A. Steinfeld, *Environ. Sci. Technol.*, 2000, **34**, 4177–4184.
21 J. Puig and M. Balat-Pichelin, *J. Magnes. Alloys*, 2016, **4**, 140–150.
22 B. A. Chubukov, A. W. Palumbo, S. C. Rowe, I. Hischier, A. J. Groehn and A. W. Weimer, *Thermochim. Acta*, 2016, **636**, 23–32.
23 L. Rongti, P. Wei and M. Sano, *Metall. Mater. Trans. B*, 2003, **34**, 433–437.
24 N. Xiong, Y. Tian, B. Yang, B. Xu, T. Dai and Y. Dai, *Vacuum*, 2019, **160**, 213–225.
25 I. Hischier, B. A. Chubukov, M. A. Wallace, R. P. Fisher, A. W. Palumbo, S. C. Rowe, A. J. Groehn and A. W. Weimer, *Sol. Energy*, 2016, **139**, 389–397.
26 I. Vishnevetsky, in *Proceedings of the ISES Solar World Congress 2015*, International Solar Energy Society, Daegu, Korea, 2016, pp. 1–12.
27 C. Yang, Y. Tian, T. Qu, B. Yang, B. Xu and Y. Dai, *Trans. Nonferrous Met. Soc. China*, 2014, **24**, 561–569.
28 N. Xiong, Y. Tian, B. Yang, B.-Q. Xu, D.-C. Liu and Y.-N. Dai, *Vacuum*, 2018, **156**, 463–468.
29 Y. Tian, B. Xu, C. Yang, B. Yang, D. Liu, T. Qu and Y. Dai, in *Magnesium Technology 2016*, eds. A. Singh, K. Solanki, M. V. Manuel and N. R. Neelameggham, John Wiley & Sons, Inc., Hoboken, NJ, USA, 2016, pp. 61–66.
30 Y. Tian, B. Xu, B. Yang, C. Yang, T. Qu, D. Liu and Y. Dai, *J. Magnes. Alloys*, 2015, **3**, 149–154.

31 R. J. Fruehan and L. J. Martonik, *Metall. Trans. B*, 1976, **7**, 537–542.
32 L. Rongti, P. Wei, M. Sano and J. Li, *Thermochim. Acta*, 2002, **390**, 145–151.
33 G. Levêque and S. Abanades, *Thermochim. Acta*, 2015, **605**, 86–94.
34 J. Puig and M. Balat-Pichelin, *J. Min. Metall. Sect. B Metall.*, 2018, **54**, 39–50.
35 B. A. Chubukov, A. W. Palumbo, S. C. Rowe, M. A. Wallace and A. W. Weimer, *Ind. Eng. Chem. Res.*, 2017, **56**, 13602–13609.
36 J. Puig and M. Balat-Pichelin, *J. Sustain. Metall.*, 2020, **6**, 161–173.
37 Y. Berro, R. Masse, J. Puig and M. Balat-Pichelin, *J. Clean. Prod.*, 2021, **315**, 128142.
38 Z. Xing, L. Bai, Y. Ma, D. Wang and M. Li, *Materials*, 2018, **11**, 1835.
39 "Peat for Fuel", *Sci. Am.*, 1858, **13** (21), 161. http://www.jstor.org/stable/24953348
40 Y. Jiang, H. W. Ma and Y. Q. Liu, *Adv. Mater. Res.*, 2013, **652–654**, 2552–2555.
41 E. S. Noumi, J. Blin and P. Rousset, in *WasteEng 2014: 5th International Conference on Engineering for Waste and Biomass Valorization*, https://agritrop.cirad.fr/574983/, Rio de Janeiro, Brazil, 2014.
42 A. Dufourny, L. Van De Steene, G. Humbert, D. Guibal, L. Martin and J. Blin, *J. Anal. Appl. Pyrolysis*, 2019, **137**, 1–13.
43 J. Deng, T. Xiong, F. Xu, M. Li, C. Han, Y. Gong, H. Wang and Y. Wang, *Green Chem.*, 2015, **17**, 4053–4060.
44 B. A. Chubukov, A. W. Palumbo, S. C. Rowe, M. A. Wallace, K. Y. Sun and A. W. Weimer, *Metall. Mater. Trans. B*, 2018, **49**, 2209–2218.
45 Y. Tian, T. Qu, B. Yang, Y.-N. Dai, B.-Q. Xu and S. Geng, *Metall. Mater. Trans. B*, 2012, **43**, 657–661.